Paleostress analysis of the Nyasa / Malawi Rift: implication for the present-day regional dynamics

Athanas S. Macheyeki[1,2] and Hassan Mdala[3]

[1] Department of Geology, College of Earth Sciences and Engineering, the University of Dodoma-Tanzania

asmacheyeki@yahoo.com

[2]Earth Sciences Institute of Shinyanga, P. O. Box 1016, Shinyanga-Tanzania

[3]Geological Survey Department of Malawi, Regional Office North, Pvt Bag 9, Mzuzu, Malawi

Abstract

The Nyasa/ Malawi rift is characterized by poor magma with relatively large earthquakes. There has been a controversy as to the stress kinematics of the rift, some considering it as part of the transform fault and some considering it as a rift structure characterized by normal faulting. To review this controversy, we collect fault slip data from the central to the southern end of the rift and integrate our results with published focal mechanisms fault slip data on the rift. Results show that the central part of the rift is under radial extension whereas the southern half is under oblique NNE-SSW transtensive tectonic regime with the horizontal axis of minimum extension = 020˚. Further south, the obliquity extension rotates by about 15˚ reaching N-S with Shmin = 175˚. The level of structural penetration and intensity of faulting show that the N-S opening is more important and prominent in the south than towards the north. We also find that the faults

that dip to the east and trending NW-SE are characterized by sinistral sense of movement whereas those that dip to the southwestern side are characterized by dextral sense of movements. This implies that regionally, the rift is essentially under normal faulting regime but with a significant strike –slip component – hence the obliquity kinematics. Tectonic regimes obtained from fault-slip data are related to lithospheric scale and involve both the crust and the upper mantle. Thus, the pure NNW-SSE extension related to focal mechanism data are crust deformation related events.

Key words: Nyasa / Malawi rift, East African Rift system, Paleostress analysis, Oblique transtensive rifting, radial extension, stress perturbation

Introduction

There are various models of rifting, major ones attest to active rifting and passive rifting (e.g. Bott, 1995; Prodehl et al., 1997; Corti et al., 2003). In the first case magma is the source of rifting where underlying magma heats the bottom of the lithosphere or the crust causing it to expand and consequently thin away and eventually leading to rifting (Buck, 1991; Bott, 1995; Gueydan et al., 2014). In the second case, no magma is involved in the rifting process (Bott, 2006; Hao et al., 2020) but that the rifting is caused by far-field stresses. There are times where both models operate (e.g. Dumond et al., 2017; Ebinger, 2020)

The East African Rift System (EARS) is one of such lithospheric scale structures whereby rifting occurs through active and passive models (e.g. Bott, 1995; Corti et al., 2003). In the process of rifting, earthquakes of various sizes occur depending on the source of the driving stresses and the

magnitude (s) of the same. Usually, deep seated earthquakes cause large to major earthquakes in rift systems. The largest recorded earthquake in rift systems are in little excess of Mw 7 ((e.g. Yan and Chen, 2010). In the EARS, the largest earthquakes Mw 7.4, struck the western branch of the EARS in SW Tanzania (Rukwa area) on December, 1910 (Ambraseys, 1991) - though others consider it to have been Mw 7.3 (Midzi and Manzunzu, 2014). It did not cause large damage at that time because most of the houses were wooden made and were scattered owing to a small population at that time. Another earthquake in that order (Ms = 7.2) occurred on 20th May, 1990 in Sudan, an areas considered to be the 350km extension of the EARS (Girdler and McConnell, 1994). The largest earthquakes within the Nyasa/Malawi rift (NMR) was in March 1989 (Mw=6.1) and December 2009 (Mw = 6.0) in Salima and Karonga respectively (Jackson & Blenkinsop, 1997). While the NMR (Fig.1) is considered to be part of the western branch of the EARS it is in part associated with magmatism to its northern part, the Rungwe volcanic province. This northern part of the NMR is associated with magma / mantle plume below (e.g. Njinju et al, 2019). The central and southern parts are magma poor (e.g. Ebinger et al., 2019; Njinju et al., 2019). While the northern part of the NMR trends NNW-SSE, the central and southern parts of the NMR trend almost N-S with local variations. Kinematics of rifting of the NMR is debatable to-date (e.g. Delvaux, et al., 1992; Ebinger et al., 2019). Chorowicz (2005) for example considers the NMR to be like a part of southern segment of the 2,100km long western branch of the EARS. Further, Chorowiciz (2005) considers the NMR to be part of the Tanganyika-Rukwa-Malawi fault zone that connects two main segments of the western branch. Using local earthquakes and source mechanisms from teleseismic earthquakes, Ebinger et al (2019) repute the NW-SE transform faulting by showing NE-SW (i.e. N58°E and N65°E) extension direction of the NMR. Similar works in support of the NE-SW extension of the

northern NMR are by Delvaux (1991), Delvaux et al. (1992), Morley (1999) and Macheyeki et al (2008). These controversies in the rifting kinematics of NMR is the main motivation for this research work.

Fig. 1-

Regional structural geological setting

The NMR is mostly underlain by Precambrian to Lower Palaeozoic Basement Complex rocks (Ray, 1975); and is located within the western branch of the EARS (Fig. 1). All the three mobile belts, Ubendian, Irumide and Mozambiquian affected the Basement Complex rocks across Malawi. Carter & Bennet (1973) identified that the three mobile belts occurred in two different tectono-metamorphic events. The first event involved the Ubendian Mobile belt from south western Tanzania, this event caused plastic deformation of the Basement Complex rocks and the second event involved both the Irumide and the Mozambiquian cycles; these two events were associated with brittle deformation of the Basement Complex rocks. Ubendian and Mozambiquian rocks dominate the Northern Province of Malawi whereas the Mozambiquian and Irumide mobile belts dominate the Southern province of the country (Carter & Bennet, 1973).

Fig. 2-

Carter & Bennet (1973) and Chapola (1997) describe tectonic structures of Malawi to be divided into two age groups namely; Pre-Cenozoic age structures and Cenozoic age structures.

The Pre-Cenozoic age structure mainly comprise those structures which were formed during the Karroo rifting of Permian to Triassic (~280 to 195 Ma) and Post Karroo rifting of Jurassic to

Cretaceous period (~195 to 65 Ma), these include faults, shear zones and dyke swarms. The Chimaliro fault zone which is to the southern side of the Champhira dome is an example of a Pre-Cenozoic structure. In southern Malawi NE-SW trending dyke swarms are examples of the Pre-Cenozoic structures.

The second group of structures comprises those structures which were formed during the Cenozoic age, these structures are associated with the initiation of the EARS, which in Malawi started about 10 million years ago. The general orientation of the rift related structures in both Northern and Southern Province of the NMR is mostly dominated by a NW-SE and N-S trending pattern with a minor NE-SW trending pattern. This, according to Delvaux, (1991) is a clear indication that the present orientation of the rift related structures is a reflection of the orogenic related structures orientation pattern most probably the Ubendian, Mozambiquian and Irumide mobile belts respectively. From this it can be deduced that the present orientation pattern of the rift related structures exist along the same orientation of the orogenic mobile belts (reactivated structures). Owing to its Z-like shaped, right-stepped pattern (Fig. 2), the NMR appears to be made of several rift segments.

Methodology

Field work for this study was undertaken in October - November 2022 over a distance of 450km beginning in the central NMR southwards. The main objective for such an endeavor was to try to unveil the stress regime sequences and kinematics of the same. Focal mechanisms data from Ebinger et al (2019) were also modeled to obtain a present day stress field and kinematics. In the field, dip amount and dip direction of fault planes with or without slickensides were measured. Those without slickensides were considered as fracture planes or joints. For the planes with slickensides, the plunge amount and plunge directions of the same were also measured. Based on

whether or not fault planes or lines (slickensides) are relatively older or younger. The basis for grouping a fault plane (and the faulting event that caused the fault plane) as younger or older was purely based on field relationship considering presence or absence of minerals, type of minerals on a given plane, cross-cutting relationship between minerals and slickensides. Different slickensides which were encountered in the field were mainly Riedel shears, mineral steps and conjugate shear fractures. After these data and information were gathered, they were then entered in a Win-Tensor software developed by Damien Delvaux and processed using the procedures described in Delvaux and Sperner (2003).

Ten sites were visited namely ERM001 to ERM010 (Fig. 2). In this Chapter, eight localities are reported ERM002-8 and ERM010. ERM001 and ERM09 had fewer data to warrant presentation here. ERM02 and ERM003 are grouped together because they occur close to each other. Similarly, ERM004 and ERM005 are grouped together because of their proximity.

Results

At Kasitu A and B, sites ERM002 and ERM003: Both sites are within a few hundred meters and just on the western lake shore (Fig. 2, 3, 4) and about 120km by road south of Mzuzu town. They both portray 2 structural orientations; NNW-SSE, N-S and NNE-SSW. Large number of the structures are fresh high-angle faults (mainly conjugated joints or shear fractures), typically cross-cutting each other at ≤60˚. Field relationship of these high-angle fracture planes indicate ENE-WSW opening of the rift.

Fig. 3 –

Fig. 4 –

In general, the fault slip data in both sites indicate three sets of fault planes; (a) sub-vertical planes with dip amounts between 75˚ and 88˚: these have sub-horizontal slip-lines <20˚, typically 6˚ to 19˚. These slip-lines indicate both sinistral and dextral shear movements-they are interpreted as strike-slip fault planes; (b) planes dipping between 54˚ and 68˚: Most of these fault planes are conjugated and oriented NW-SE. They are interpreted as normal fault planes indicating rift opening in an ENE-WSW; and (c) shallow – angle dipping planes (approximately 40˚): These fault planes are oriented NE-SW. Direction of movement in one of the slip lines on these fault planes is NE-SW (i.e. 39˚ towards 028˚). These types of faults are showing oblique opening along NE-SW, sub-parallel to the orientation of the fault planes themselves.

It can be summarized therefore that opening of the rift at both Kasitu A and B is ENE-WSW and NE-SW regardless of the type of structures in which the movement is occurring. Modelled stress tensor for these sites indicate normal faulting regime with radial extension stress regime with Shmin=151˚, SHmax = 061˚ (Fig. 3, Table 1).

Table 1 –

At Diwangu and Bua rivers, sites ERM004 and ERM005 (Fig. 5): These points are located 60m from Kasitu sites along the lake shore. Unlike ERM002 and ERM003 at Kasitu, ERM004 and ERM005 are characterized by two fault trends; NW-SE and NNW-SSE. The main fault planes are high-angle faults, typical of strike-slip faults and are oriented in such a way that those faults that dip to the east and trending NW-SE are characterized by sinistral sense of movement whereas those that dip to the southwestern side are characterized by dextral sense of movement (Fig. 6). Foliation fabric of the Precambrian basement measured here dip 40˚ towards 220˚.

Fig. 5 –

Fig. 6-

At Kazipuru river bridge: site ERM006: This site is located on the southern part of the NMR (Fig. 2, 3, 6). It is characterized by NW-SE trending faults which are the major ones here. NE-SW trending faults are also present but comparably less pronounced than the former. There are also W-E trending faults. While all the three sets of faults seem to be relatively younger (i.e. Cenozoic), the W-E trending faults seem to be the youngest owing to their fresher surfaces and echelon pattern in most places, typical of isolated fault strands. The E-W faults are less penetrative, probably restricted to upper crust tectonics.

In the same site are E-W trending thrust faults. The planes of movement are associated with quart-hornblende minerals implying that they are the oldest faults in the area. A pervasive brittle deformation in the area is exemplified by fault breccia, most likely related to Karoo rifting. The thrust faults are also attributed the Karoo tectonics. In the same area are tight folds, characterized by NNW-SSE trending axial plane. These ductile-semi ductile deformation structures seem to have been formed by NNE-SSW compressive stress field. In summary, the tectonic events in the area are as follows: (a) metamorphism of the Precambrian basement, (b) folding of the basement, (c) thrusting associated with quartz-hornblende mineralization, (d) faulting associated with breccia, (e) recent deformation associated with the barren faults (strike slip and normal faults)-of all these the E-W faults are the youngest (Fig. 8a, b). The overall stress field from modelled stress tensor corresponding to the present stress kinematics is shown in Figure 3. It is characterized by an oblique transtensive stress field oriented NNE-SSW with Shmin=020˚, SHmax= 110˚.

Fig. 7 –

Fig. 8a –

Fig. 8b-

About 10km south of Kazipuru river is the Mua site, ERM007 (Fig. 2, 3, 9). This is a place where a fresh cut of a fault scarp is observed. Water falls on the scarp in such a way that one can visualize the recent faulting. Most of the faults here are high-angle faults meaning that the normal fault related scarp was formed from reactivation of strike-slip faults. Few measurements taken at this point indicate that the fault planes dip between 68˚ and 74˚ and the slip lines show block movements at 40˚ dip amount towards NW (336˚).

Nearly 80km SE of this site is the Malombe site. It is located just east of the Malombe fault and west of Lake Malombe. Like for most fault planes in this area, the fault planes here are mostly high-angle faults 70˚ to sub-vertical, generally dipping to the north and NNE. The prominent structures at Malombe site are the NNW-SSE that dip due north to NNE. Slip vectors along the fault planes vary from N to E, meaning that there are faults that open in a N-S direction and those that open in an E-W direction. The latter are less prominent whereas the faults that open in a N-S direction are prominent and are more deep seated than at Kazipuru site (ERM006).

On the western site of Malombe site where the Malombe fault is located, landslide is clear. This landslide has affected most of the rocks units and has equally disturbed the orientation of the structures on the hanging wall side including the structures at the Malombe site (ERM008).

Fig. 9 –

At Twabwa Quarry: site ERM010: This site is more than 200km by road south of ERM008. It is along the NW-SE trending Chyolo active fault (Fig. 2, 3,10).

Both dip slip and lateral movements characterize this fault and both components seem to occur together in any given plane. The prominent sense of movement in all the faults in this southern

most part of the rift is sinistral. Three types of faults are recognized from their planes and slip movements; normal faults, strike-slip and thrust faults. The latter is quartz veined and therefore older than the normal and strike slip faults (the barren ones). The oldest tectonic structures in the area are the S-C fabrics associated with Precambrian deformational events. The modelled stress tensor corresponding to the most recent rifting stress field is presented in Figure 3. It indicates that this southernmost part of the NMR is opening obliquely along the N-S direction. Comparing site ERM006, ERM008 and ERM010 in terms of level of N-S opening slickensides, it is evident that the magnitude is increasing southerly. The slickensides and the fault planes in which they occur are clearer as one moves from central part of the NMR to the southern part (i.e. from ERM006 to ERM010, Fig. 11).

Fig. 10 –

Fig. 11-

Discussion

According to Daly (1998), the NW-SE trending Precambrian Ubendian structures are ductile to semi-ductile shear zones and folds. These are intersected by NE-SW trending Karoo shear zones and faults (Normal and strike-slip faults such as the Ruhuhu, Ruangwa and Maniamba troughs (e.g. Njinju et al. 2019). The zones of intersections were, and are still the weakest structural zones in the entire rift subject of future fault reactivation and locus of deep seated magmatism.

Delvaux et al (1992) and Njinju et al (2019) show that the Cenozoic rifting reactivated Precambrian structures (shear zones). According to Delvaux et al. (1992), the reactivation in Late Miocene to Pleistocene was a near radial extensive regime and was followed by strike-slip faulting (compressive regime) in the Late Pleistocene. Both the Late Miocene-Pleistocene and

the Late Pleistocene tectonic events were associated with the magmatic pulses in the Rungwe volcanic province.

This work has demonstrated five major findings from fault slip data collected from the central part to the southern part of the NMR:

First of all; the central part is under radial extension. This is compatible with the Late Miocene-Pleistocene rifting model reported by Delvaux et al (1992) for the northern part of the NMR. Such results indicate that the radial extension is from the central part to the northern part of the rift. Radial extension means opening of the rift in all directions- a phenomenon that is attributed to plume activities or lithospheric scale magmatic activities (e.g. Reiss et al., 2021). Second; the southern half of the NMR is under oblique NNE-SSW transtensive tectonic regime with Shmin = 020˚. Third; further south, the obliquity extension rotates by about 15˚ reaching N-S direction with Shmin = 175˚ (Table 1, Fig. 3). Type localities for this N-S extension phenomena were recorded in Kazipuru river (ERM006), Malombe fault (west of Lake Malombe, ERM008) and Twabwa area along the Thyolo fault (ERM010). Forth; the level of structural penetration and intensity of faulting show that the N-S opening is more pronounced in the south than towards the north, and fifth; the faults that dip to the east and trending NW-SE are characterized by sinistral sense of movement whereas those that dip to the southwestern side are characterized by dextral sense of movements. It implies that the rift is essentially under normal faulting regime but with a significant strike –slip component – hence the obliquity kinematics.

As most of the data collected on the Malawi side indicate that fault planes dipping to the east have sinistral sense of movement as contrasted by the fault planes dipping to the western side which have dextral sense of movement, it implies that most of the faults in Malawi (i.e. middle

and southern part) are under sinistral oblique faults and the faults in the northern segment that dips to the west are under dextral sense of movements.

Modeled stress tensors from focal mechanism data compiled by Ebinger et al. (2019) for small to moderate earthquakes that occurred in the last half a century (1968 to 2019) consistently indicate a pure extension regime oriented NNW-SSE (Shmin = 165), implying normal faulting events only. However, looking at individual seismic data for the area, strike-slip events are present, and though are few, they are generally related to over 30km deep events meaning that they are related to the lithospheric segments. As most of the reported seismic events in the area for the last 50 years are small to moderate, it appears that they are related to shallow seated events, most likely upper crust faulting events. It should be noted that, small to moderate earthquakes whether magmatic or tectonic in origin or both, are generally not able to leave a mark on the rocks (McCalpin, 1996; Keller and Pinter 2002**)**. In other words, earthquakes larger than moderate earthquakes are the ones that can leave marks (slickenlines) on rocks and that fault slip data are the ones related to large earthquakes. It has to be made clear here that even the upper crustal tectonic activities can cause large earthquakes and small earthquakes may come from middle to lower crust (Yang and Chen, 2010).

Putting both fault slip and focal mechanism data into regional perspective, it can be implied that, the NMR has not been deforming in the same way both in time and space. During the Late Pleistocene, the lithospheric scale deformation assisted by mantle plume, affected the middle to northern part of the rift which is magma rich causing it to open radially. This explains why the middle / central part of the NMR are under radial extension. Delvaux et al (1992) also report radial extension related to Miocene – Pleistocene. It means that this event continued to Late Pleistocene or even to Holocene and is still ongoing or was repeated some thousand years before

present (episodic rifting). During the same time (Late Pleistocene to Holocene), the southern part was opening obliquely under the so called oblique NNE-SSW transtensive regime and further to the southern end, it was opening in an oblique N-S extensive regime.

It is though difficult to comprehend a N-S extension within a generally N-S oriented NMR. Owing to freshness of the N-S opening structures (Fig. 8) and the relatively less penetrative field relationship, it can be implied that these structures are related to upper crust deformation activities which are related to secondary faults (e.g. Maerten et al., 2002) developed by local stress perturbations (e.g. Maerten et al., 2002; Chen et al., 2008; Feng et al., 2020) in the process of rifting caused by active / and far field stresses. Stress perturbations, and hence changes of positions of the principal stress axis σ_1 can occur as a result of pre- and post- seismic stress states differences (e.g. Hasegawa et al., 2012; Yoshida et al., 2014; Feng et al., 2020) and pore pressure changes (e.g. An eta l., 2021). As the NMR is still a younger rift and more particularly towards its southern tip, it is not surprising to find these intra basinal sub-orthogonal structures to the rift being developed (e.g. Fig. 8a, b) and are more important towards the southern (relatively youngest) tip of the rift (Fig. 11).

Conclusion

The northern to middle part of the NMR is under radial to sub-radial extension because of both tectonic and possibly magma activities. The southern part of the rift is opening obliquely in the NNE-SSW to N-S. The latter kinematics is considered to be attributed to stress perturbations at the upper crustal level, the process that is actively ongoing in the NMR. Therefore, the actual active regional opening direction of the NMR to its southern part, hereby reported is NNE-SSW characterized by an oblique transtensive stress field with Shmin = 020˚ and R′ = 1.91 meaning

290 that faulting / rifting has both normal and strike-slip components. This NNE-SSW extensional
291 direction for the NMR obtained from this work is somewhat in disagreement with some of the
292 published extensional directions that attests to NE-SW directions (e.g. Ebinger et al, 2019,
293 extension direction N58°E and N65°E) and NW-SE (e.g. Ring and Betzler; 1995; Chorowicz,
294 2005).

295

296

297

298

299 **References**

300 Ambraseys, N.N. (1991). The Rukwa earthquake of 13 December 1910 in East Africa. Terra
301 Nova, 3(2), 202–211. doi:10.1111/j.1365-3121.1991.tb00873.x

302 An, M., Zhang, F., Dontsov, E., Elsworth, D., Zhu, H. & Zhao, L. (2021). Stress perturbation
303 caused by multistage hydraulic fracturing: Implications for deep fault reactivation.
304 International Journal of Rock Mechanics and Mining Sciences, 141,
305 104704. doi:10.1016/j.ijrmms.2021.104704

306 Bott, M.H.P. (1995). Mechanisms of rifting: geodynamic modeling of continental rift systems.
307 *In*: Olsen, K.H. (Ed.), Continental Rifts: Evolution, Structure, Tectonics. Elsevier Series:
308 Amsterdam, 409-436p.

309 Bott, M.H.P. (2006). Mechanisms of rifting: Geodynamic modeling of continental rift systems.
310 Developments in Geotectonics, 27–43. doi:10.1016/s0419-0254(06)80006-6

311 Buck, W.R. (1991). Modes of continental lithospheric extension. Journal of Geophysical
312 Research, B, Solid Earth and Planets 96(12), 20161–20178.

313 Carter, G.S. & Bennet, J.D. (1973). The Geology and Mineral Resources of Malawi.

314 Chapola, L. (1997). State of stress in East and Southern Africa and Seismic Hazard Analysis of
315 Malawi [Institute of Solid Earth Physics, University of Bergen, Norway (MSc Thesis).].
316 http://www.researchgate.net/post/How_do_I_extract_lineaments_from_Landsat_Image_and
317 _RADAR

318 Chen, Y.Z., Lin, X.Y. & Wang, Z.X. (2008). T-stress evaluation for slightly curved crack using
319 perturbation method. International Journal of Solids and Structures 45, 211–224

320 Chorowicz, J. (2005). The East African rift system. J. Afr. Earth Sci. 43, 379-410

321 Corti, G., Bonini, M., Conticelli, S., Innocenti, F., Manetti, P. & Sokoutis, D. (2003). Analogue
322 modelling of continental extension: A review focused on the relations between the
323 patterns of deformation and the presence of magma, Earth Sci. Rev., 63, 169 – 247.
324 https://doi.org/10.1016/S0012-8252(03)00035-7

325 Delvaux, D. (1991). The Karoo to recent rifting in the western branch of the East-African Rift
326 System: a bibliographical synthesis. Musee Roy. Afr. Central Tervuren (Dép. Géol. Min.,
327 Rap. Ann.) 1989–1990, 63–83.

328 Delvaux, D. & Sperner, B. (2003). Stress tensor inversion from fault kinematic indicators and
329 focal mechanism data: the TENSOR program. *In*: Nieuwland, D. (Ed.), New Insights into

330 Structural Interpretation and Modelling, vol. 212. Geological Society of London, Special
331 Publication, pp. 75–100.
332 Delvaux, D. & Barth, A. (2010). African stress pattern from formal inversion of focal
333 mechanism data. Implications for rifting dynamics. Tectonophysics 482, 105– 128.
334 Delvaux, D., Levi, K., Kajara, K. & Sarota, S. (1992). Cenozoic Paleostress and Kinematic
335 Evolution of the Rukwa - North Malawi Rift Valley (East African Rift System). Bulletin
336 du Centre de Recherches elf Exploration Production elf Aquitaine (16/2), 383–406.
337 Win-tensor software by Damien Delvaux of 5th October, 2021. (Version 5-9-2) [Dataset].
338 https://www.damiendelvaux.be/Tensor/WinTensor/win-tensor_download.html
339 Feng, C., Yang, Y., Ma, X., Qi, B., Zhang, P., Meng, J., Tan, C. & Chen, Q. (2020). Local stress
340 perturbations associated with the 2008 Wenchuan M 8.0 earthquake near the
341 Longmenshan fault zone in the eastern margin of the Tibetan Plateau. Journal of Asian
342 Earth Sciences, 200, 104429. doi:10.1016/j.jseaes.2020.104429
343 Girdler, R. W. & McConnell, D.A. (1994). The 1990 to 1991 Sudan Earthquake Sequence and
344 the Extent of the East African Rift System. Science, 264(5155), 67–
345 70. doi:10.1126/science.264.5155.67
346 Gueydan, F. & Précigout, J., 2014. Modes of continental rifting as a function of ductile strain
347 localization in the lithospheric mantle. Tectonophysics, 612-613, 18–
348 25. doi:10.1016/j.tecto.2013.11.029
349 Hasegawa, A., Yoshida, K., Asano, Y., Okada, T., Linuma, T. & Ito, Y., 2012. Change in stress
350 field after the 2011 great Tohoku-Oki earthquake. Earth Planet. Sci. Lett. 355–356, 231–
351 243.

352 Hao, L., Loon, A.J.V., Xu, J., Tian, L. & Chen, D. (2020). Relationships between tectonic
353 activity and sedimentary source-to-sink system parameters in a lacustrine rift basin: a
354 quantitative case study of the Huanghekou Depression (Bohai Bay Basin, East China).
355 Basin Res. 32, 587–612.

356 Jackson, J. & Blenkinsop, T. (1997). The Bilila-Mtakataka fault in Malaŵi: An active, 100-km
357 long, normal fault segment in thick seismogenic crust. Tectonics, 16(1), 137–150.
358 https://doi.org/10.1029/96TC02494

359 Keller, A. & Pinter, N. (2002). Active tectonics. Earthquakes, Uplift and Landscape. 2d ed.
360 Prentice Hall Earth Sciences Series: New Jersey, 362pp.

361 Macheyeki, A.S., Mdala, H., Chapola, L.S., Manhiça, V.J., Chisambi, J., Feitio, P., Ayele, A.,
362 Barongo, J., Ferdinand, R. W., Ogubazghi, G., Goitom, B., Hlatywayo, J. D., Kianji, G. K.,
363 Marobhe, I., Mulowezi, A., Mutamina, D., Mwano, J. M., Shumba, B. & Tumwikirize, I.
364 (2015). Active fault mapping in Karonga-Malawi after the December 19, 2009 Ms 6.2
365 seismic event. Journal of African Earth Sciences, 102, 233–246.
366 https://doi.org/10.1016/j.jafrearsci.2014.10.010

367 Macheyeki, A.S., Delvaux, D., De Batist, M. & Mruma, A. (2008). Fault kinematics and tectonic
368 stress in the seismically active Manyara-Dodoma rift branch in Central Tanzania –
369 Implications for the East African Rift. J. Afr. Earth Sci. 51, 163–188.

370 Maerten, L., Gillespie, P. & Pollard, D.D. (2002). Effects of local stress perturbation on
371 secondary fault development. Journal of Structural Geology 24, 145-153.

372 McCalpin, J.P. (Ed.) (1996). Paleoseismology. Academic Press: New York, 583pp.

373 Midzi, V. & Manzunzu, B. (2014). 15 - Large recorded earthquakes in sub-Saharan Africa. Part
374 IV - Case studies: Africa. Cambridge University Press:

375 Prodehl, C., Fuchs, K. & Mechie, J. (1997). In: Structure and dynamic processes in the
376 lithosphere of the Afro-Arabian rift system. Ed.: K. Fuchs. Amsterdam 1997. S. 1-13.
377 (Tectonophysics. 278,1/4.)

378 Ray, G.E. (1975). The Geology of the Chitipa - Karonga Area.
379 http://www.bgs.ac.uk/research/highlights/2010/malawiMineralPotential.html

380 Reiss, M.C., Muirhead, J.D., Laizer, A.S., Link, F., Kazimoto, E.O., Ebinger, C.J. & Rümpker,
381 G. (2021). The impact of complex volcanic plumbing on the nature of seismicity in the
382 developing magmatic Natron rift, Tanzania Miriam Christina. Front. Earth Sci., 23 Sec.
383 Volcanology. https://doi.org/10.3389/feart.2020.609805

384 Ring, U. & Betzler, C. (1995). Geology of the Malawi Rift: kinematic and tectonosedimentary
385 background to the Chiwondo Beds, northern Malawi. Journal of Human Evolution, 28(1),
386 7–21. doi:10.1006/jhev.1995.1003

387 Shillington, D. (2010). Continental Breakup in East Africa – State of the Planet.
388 http://blogs.ei.columbia.edu/2010/02/05/continental-breakup-in-east-africa/

389 Yang, Z., & Chen, W.-P. (2010). Earthquakes along the East African Rift System: A multiscale,
390 system-wide perspective, J. Geophys. Res., 115, B12309, doi:10.1029/2009JB006779

391 Yoshida, K., Hasegawa, A., Okada, T. & Linuma, T. (2014). Changes in the stress field after the
392 2008 M 7.2 Iwate-Miyagi Nairiku earthquake. J. Geophys. Res. Solid Earth 119, 9016–
393 9030.

394

List of Figures

Table 1: – Stress tensor parameters obtained from fault slip data and focal mechanisms for the NMR. (n): number of data used in the inversion, (nt): total number of data in the database, (σ_1, σ_2 and σ_3) are the principal

stress axes, i.e. maximum, intermediate and minimum respectively, (R): stress ratio, (QRw): quality rank, (R'): stress regime index, (Reg): stress regime according to the World Stress Map, (SHmax, Shmin): respectively, maximum and minimum horizontal principal stress directions. (σ mag): normal stress magnitude, (τ mag): shear stress magnitude and (Θ) the angle between normal and shear stress

Acknowledgements

This mission was made possible through the warm collaboration between the Geological Survey Department of Malawi (MGSD). We particularly thank Mr. Kondwani Dombola, the Acting Director of the MGSD for accepting the request of the first author to work with the Survey. The MGSD made available to the researchers, the resources such as data, field vehicle and organized for field logistics throughout the time we were in Malawi. We are indebted to Mr. Patrick Chindandali and Mr Yohane Kaukutu (Librarian) both from MGSD for making available to us some literatures useful for our work. Special thanks to Rebeka B. Mwakalinga from Tanzania for joining us in the field. Mr Benjamin Chirwa provided a safe and warm driving throughout the fieldwork. We also thank each and every one who in one way or another supported us.

Paleostress analysis of the Nyasa / Malawi Rift: implication for the present-day regional dynamics

Athanas S. Macheyeki[1,2] and Hassan Mdala[3]

[1] Department of Geology, College of Earth Sciences and Engineering, the University of Dodoma-Tanzania

asmacheyeki@yahoo.com

[2]Earth Sciences Institute of Shinyanga, P. O. Box 1016, Shinyanga-Tanzania

[3]Geological Survey Department of Malawi, Regional Office North, Pvt Bag 9, Mzuzu, Malawi

Table 1 –

Site ID	Location	n	nt	σ_1	σ_2	σ_3	R	R'	SHmax	Shmin	Regime	Stress Regime	Θ	σ mag	τ mag	QRw
ERM002/3	Kasitu A/B	6	12	80/168	02/064	10/333	0.2	0.2	61	151	NF	Radial EXTENSIVE	24.8	30.4	16	D
ERM006	Kazipuru river	11	11	39/108	41/333	25/220	0.09	1.91	110	20	NS	Oblique TRANSTENSIVE	38.5	37.7	31.7	C
ERM010	Thabwa-(Thyolo Fault)	6	7	50/250	35/104	17/001	0.54	0.54	85	175	NS	Oblique EXTENSIVE	35.7	42.5	26.8	D
Focal Mechanisms-All data		112	188	88/176	00/075	02/345	0.36	0.36	75	165	NF	Pure EXTENSIVE	35.7	54.7	36.6	A
Focal mechanisms – Northern		62	126	82/135	03/246	08/336	0.41	0.41	73	163	NF	Pure EXTENSIVE	34.7	53.4	34.4	A
Focal mechanisms – Southern	FM data	71	80	80/069	10/253	01/163	0.28	0.28	67	157	NF	Pure EXTENSIVE	37.8	55	40.2	A

Figure 1.

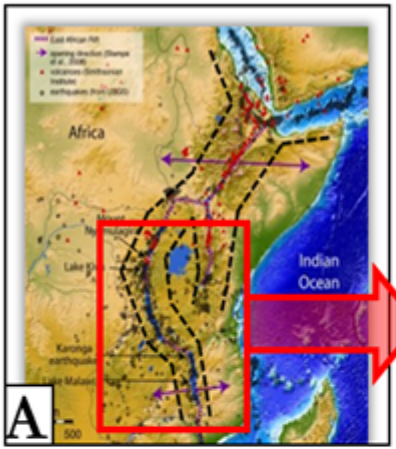
Africa
Indian Ocean
A

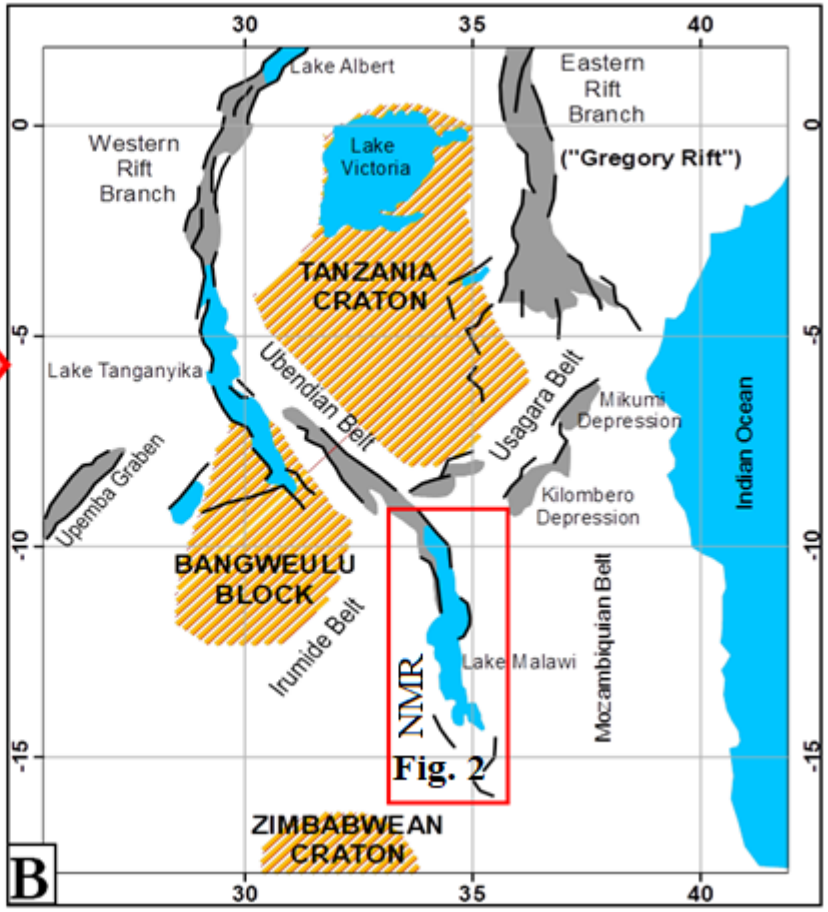
30
35
40
0
-5
-10
-15
Lake Albert
Eastern Rift Branch
("Gregory Rift")
Western Rift Branch
Lake Victoria
TANZANIA CRATON
Lake Tanganyika
Ubendian Belt
Usagara Belt
Mikumi Depression
Kilombero Depression
Indian Ocean
Upemba Graben
BANGWEULU BLOCK
Irumide Belt
NMR
Lake Malawi
Mozambiquian Belt
Fig. 2
ZIMBABWEAN CRATON
B

Figure 2.

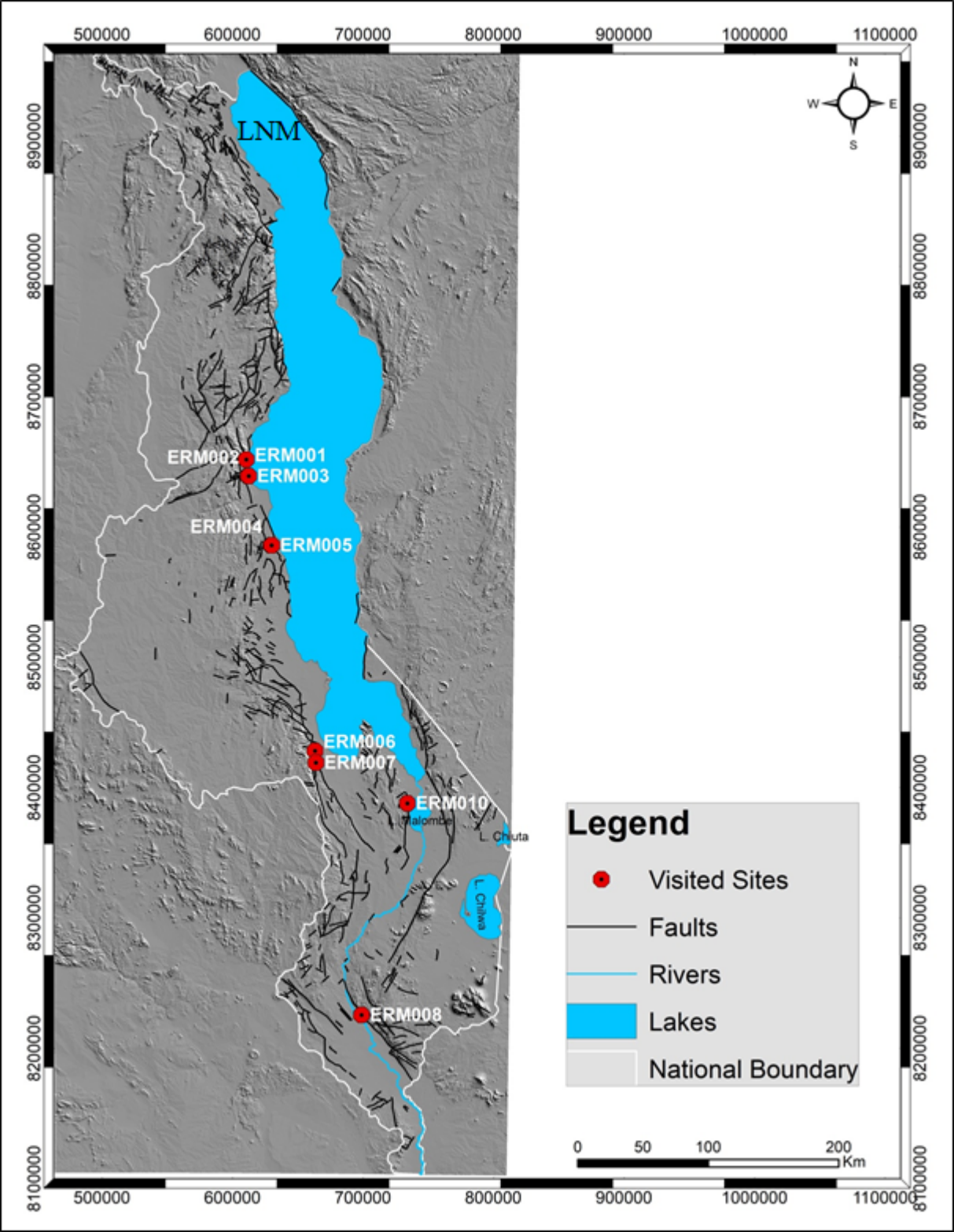
500000
600000
700000
800000
900000
1000000
1100000
8900000
8800000
8700000
8600000
8500000
8400000
8300000
8200000
8100000
N
W
E
S
LNM
ERM002
ERM001
ERM003
ERM004
ERM005
ERM006
ERM007
ERM010
Malombe
L. Chiuta
L. Chilwa
ERM008
Legend
Visited Sites
Faults
Rivers
Lakes
National Boundary
0
50
100
200
Km

Figure 3.

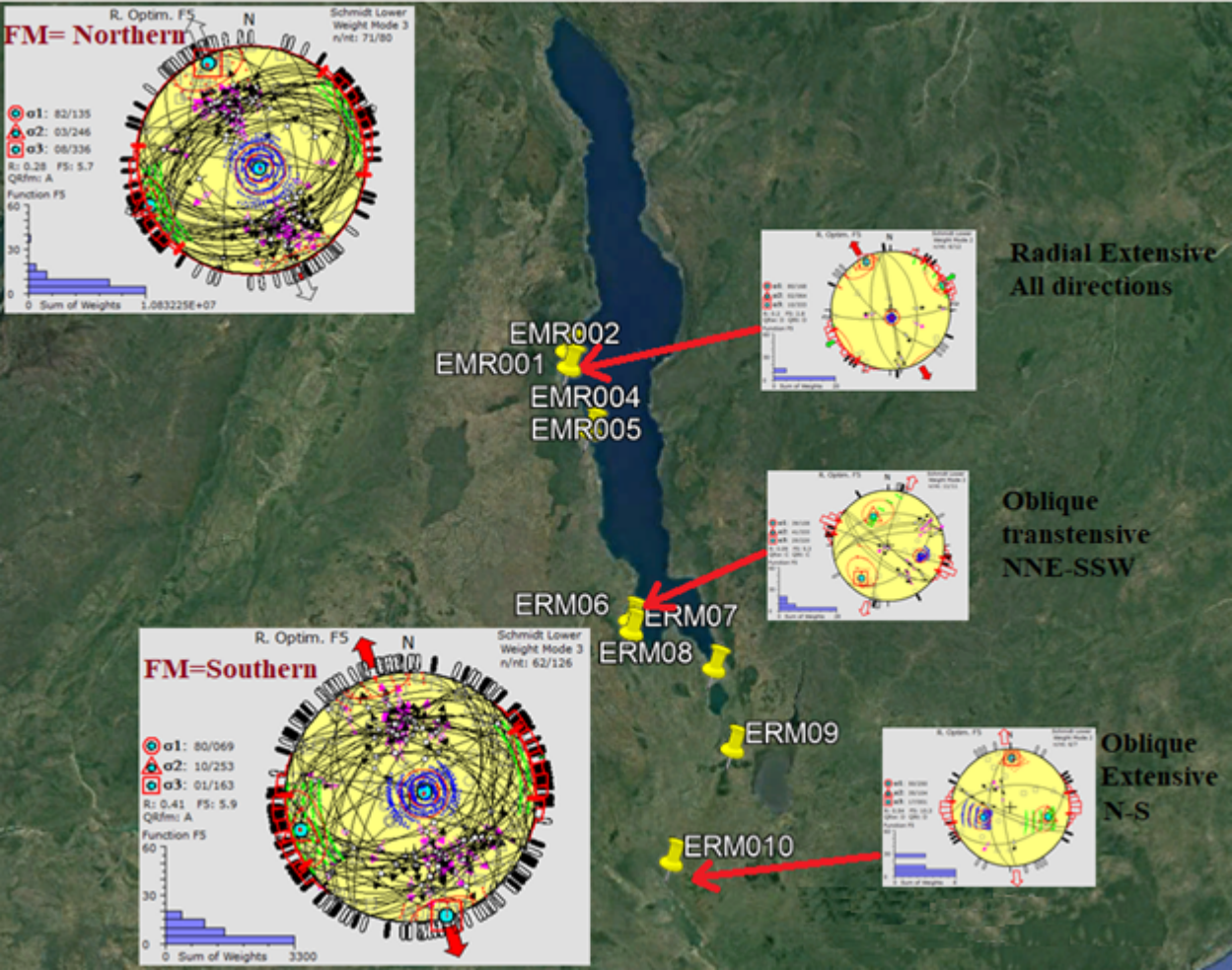
FM= Northern
R. Optim. FS
N
Schmidt Lower
Weight Mode 3
n/nt: 71/80
σ1: 82/135
σ2: 03/246
σ3: 08/336
R: 0.28 FS: 5.7
QRfm: A
Function FS
60
30
0
0 Sum of Weights 1.083225E+07
Radial Extensive
All directions
EMR002
EMR001
EMR004
EMR005
Oblique
transtensive
NNE-SSW
ERM06
ERM07
ERM08
ERM09
ERM010
Oblique
Extensive
N-S
FM=Southern
R. Optim. FS
N
Schmidt Lower
Weight Mode 3
n/nt: 62/126
σ1: 80/069
σ2: 10/253
σ3: 01/163
R: 0.41 FS: 5.9
QRfm: A
Function FS
60
30
0
0 Sum of Weights 3300

Figure 6.

Northern rift (segment)

Dextral sense of movement on westerly dipping faults / fault planes (both dip and lateral movements occur)

Southern rift (segment)

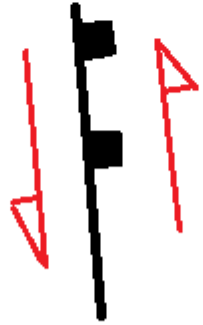

Sinitral sense of movement on easterly dipping faults / fault planes (both dip and lateral movements occur)

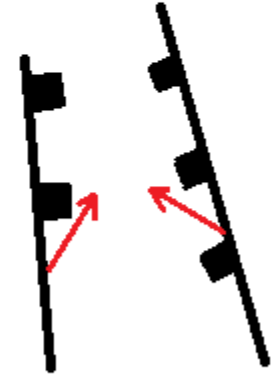

Effective transport of materials

Figure 8b.

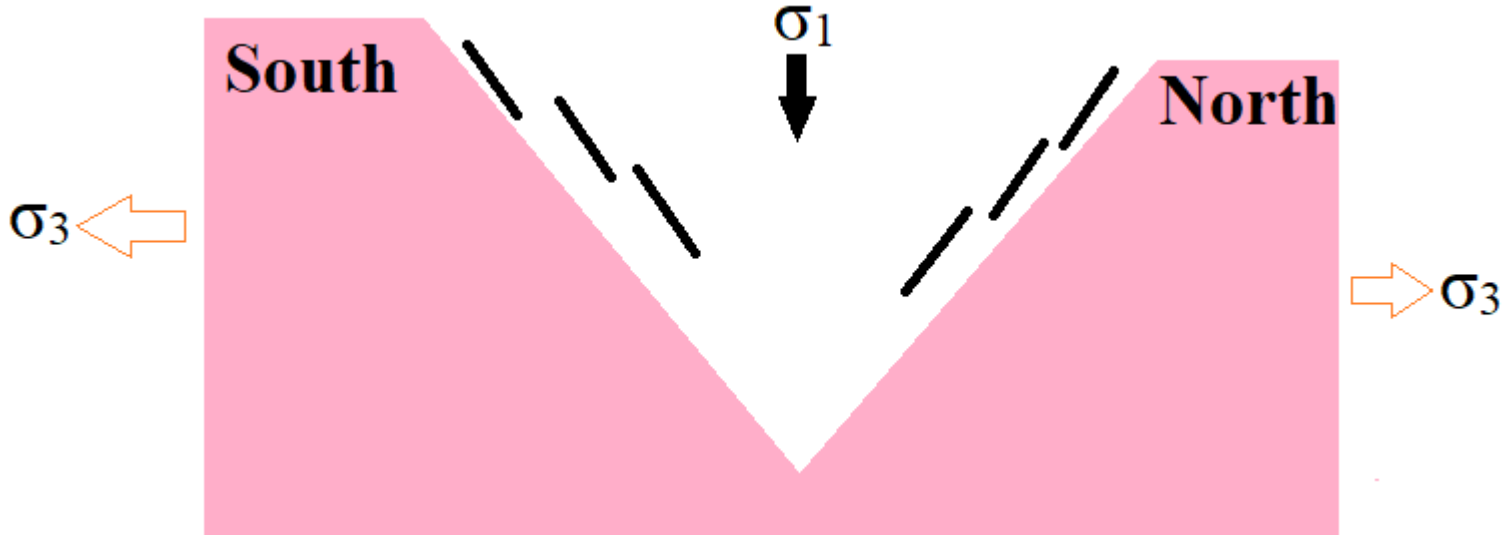
South
North
σ1
σ3
σ3

Figure 8a.

Figure 11.


FBM610

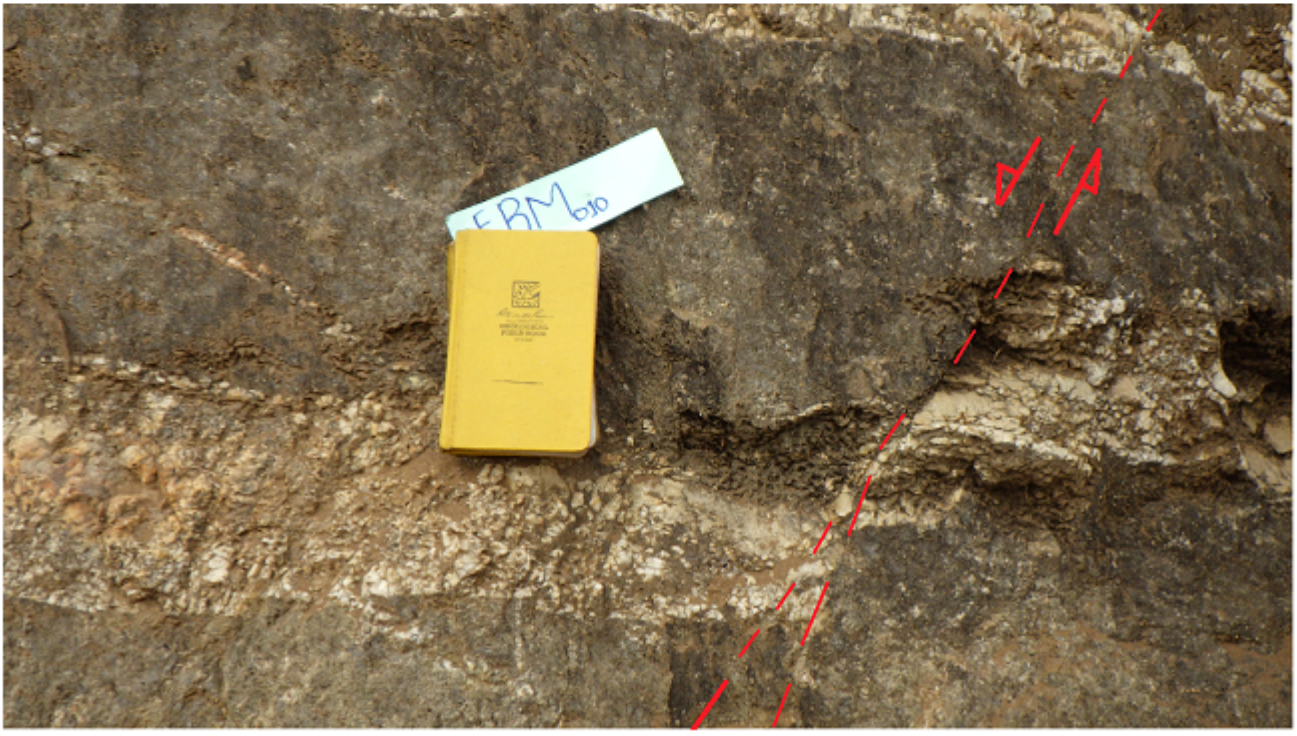
FBM610
A
A

Figure 4.

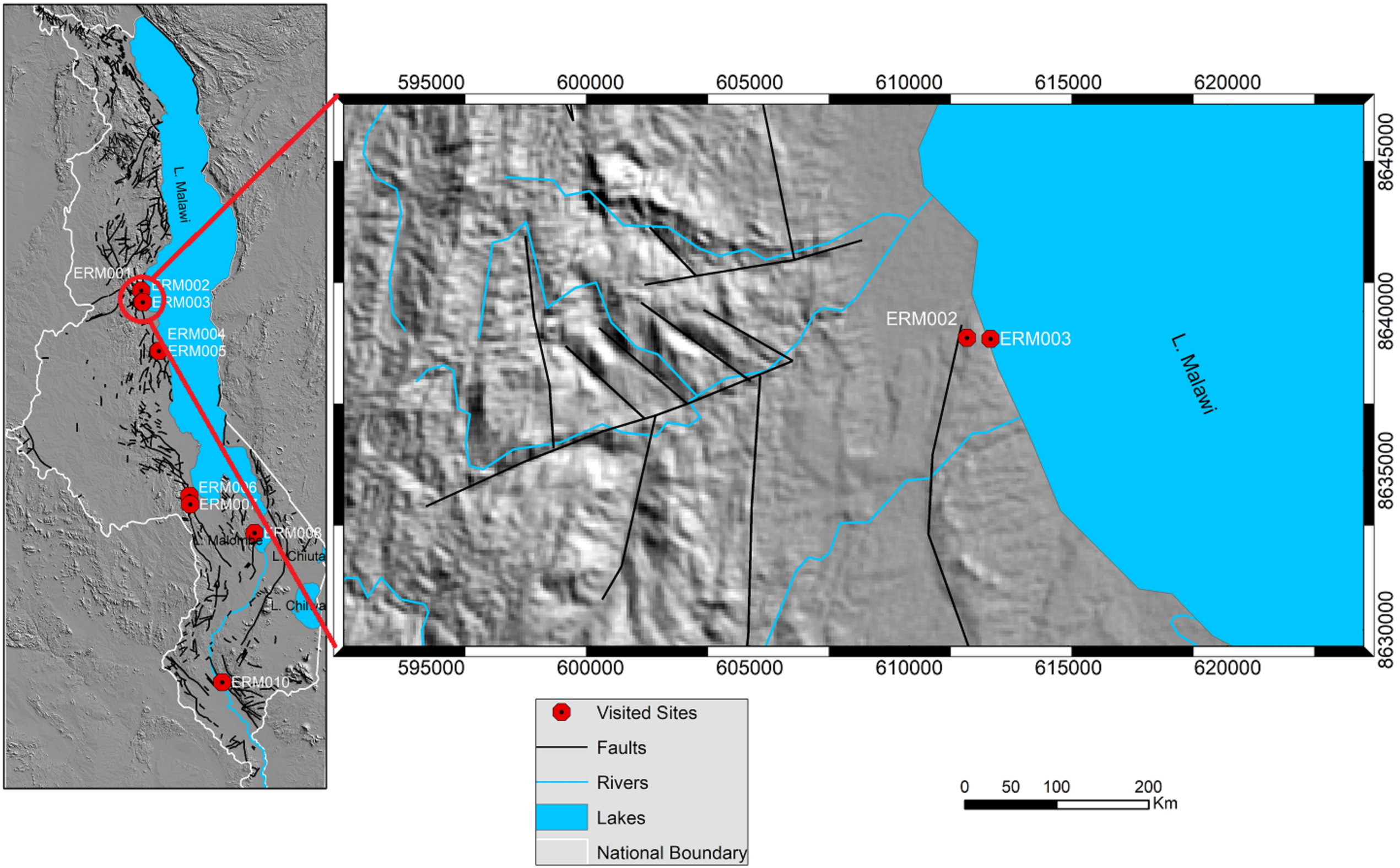
N
W
E
S
595000
600000
605000
610000
615000
620000
8645000
8640000
8635000
8630000
L. Malawi
ERM001
ERM002
ERM003
ERM004
ERM005
ERM006
ERM007
ERM008
L. Malombe
L. Chiuta
L. Chilwa
ERM010
Visited Sites
Faults
Rivers
Lakes
National Boundary
0 50 100 200
Km

Figure 7.

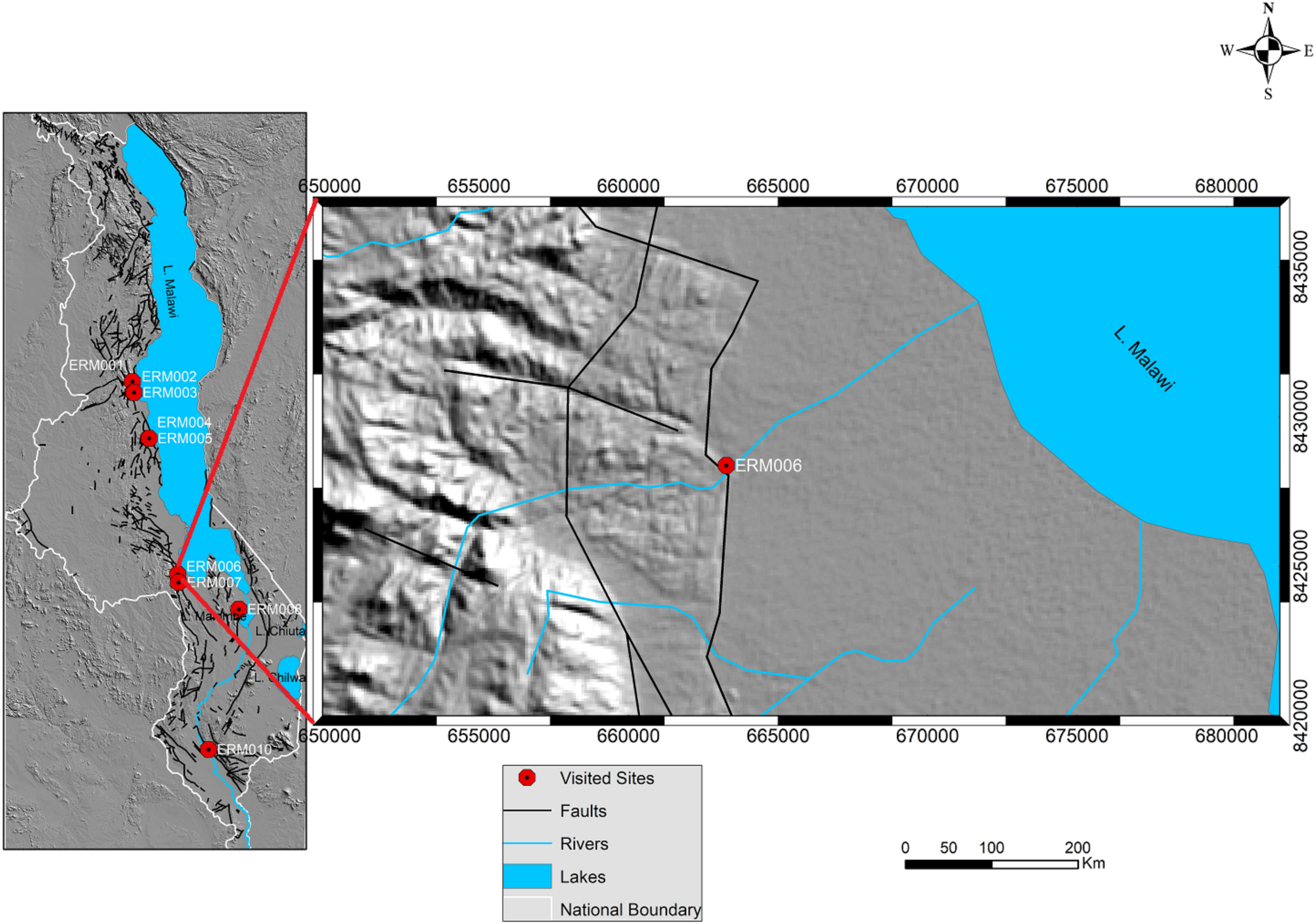
N
W
E
S
L. Malawi
ERM001
ERM002
ERM003
ERM004
ERM005
ERM006
ERM007
ERM008
ERM010
L. Chiuta
L. Chilwa
650000
655000
660000
665000
670000
675000
680000
8435000
8430000
8425000
8420000
Visited Sites
Faults
Rivers
Lakes
National Boundary
0
50
100
200
Km

Figure 5.

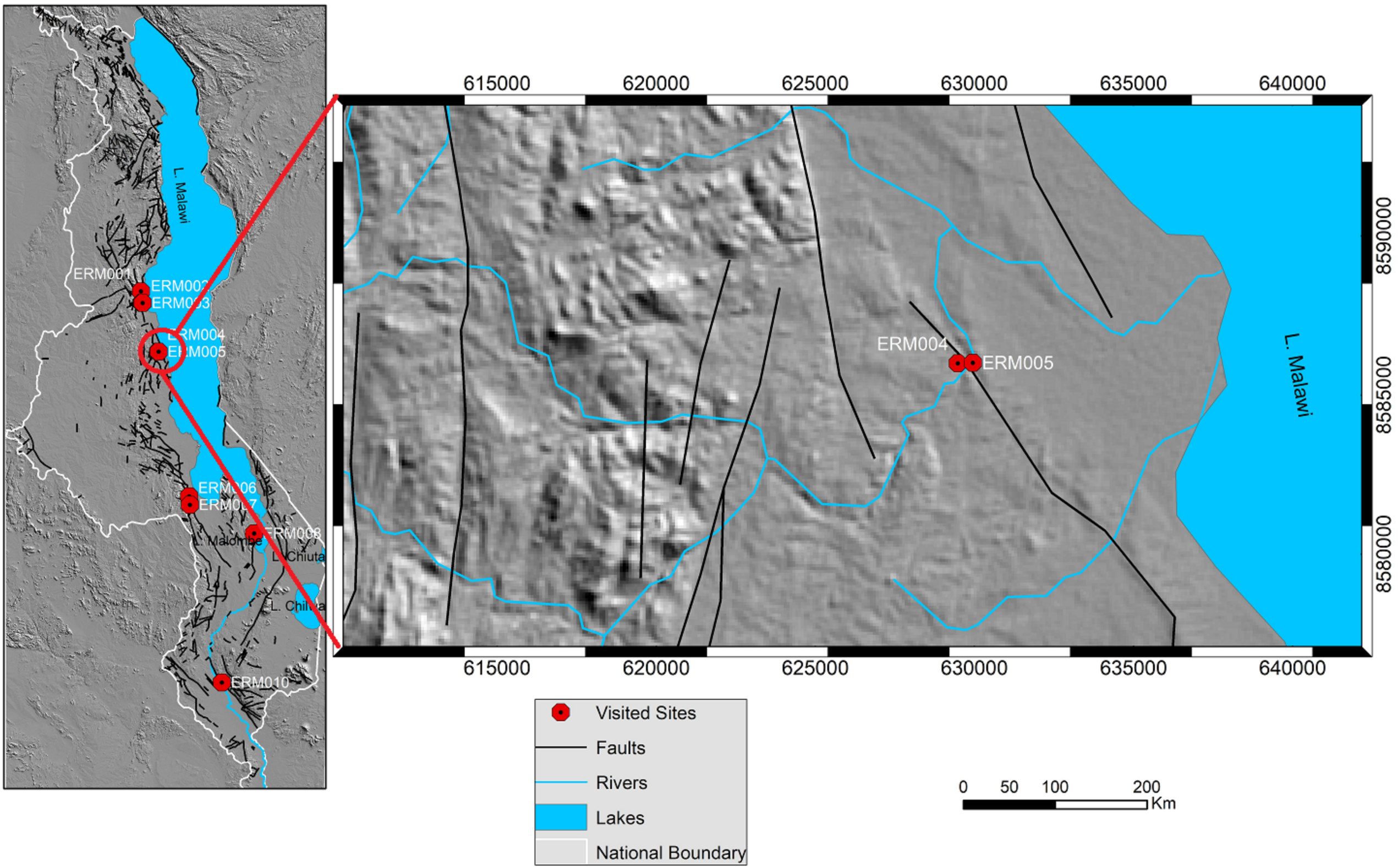
N
W
E
S
615000
620000
625000
630000
635000
640000
8590000
8585000
8580000
L. Malawi
ERM001
ERM002
ERM003
ERM004
ERM005
ERM006
ERM007
ERM008
L. Malombe
L. Chiuta
L. Chilwa
ERM010
Visited Sites
Faults
Rivers
Lakes
National Boundary
0 50 100 200
Km

Figure 9.

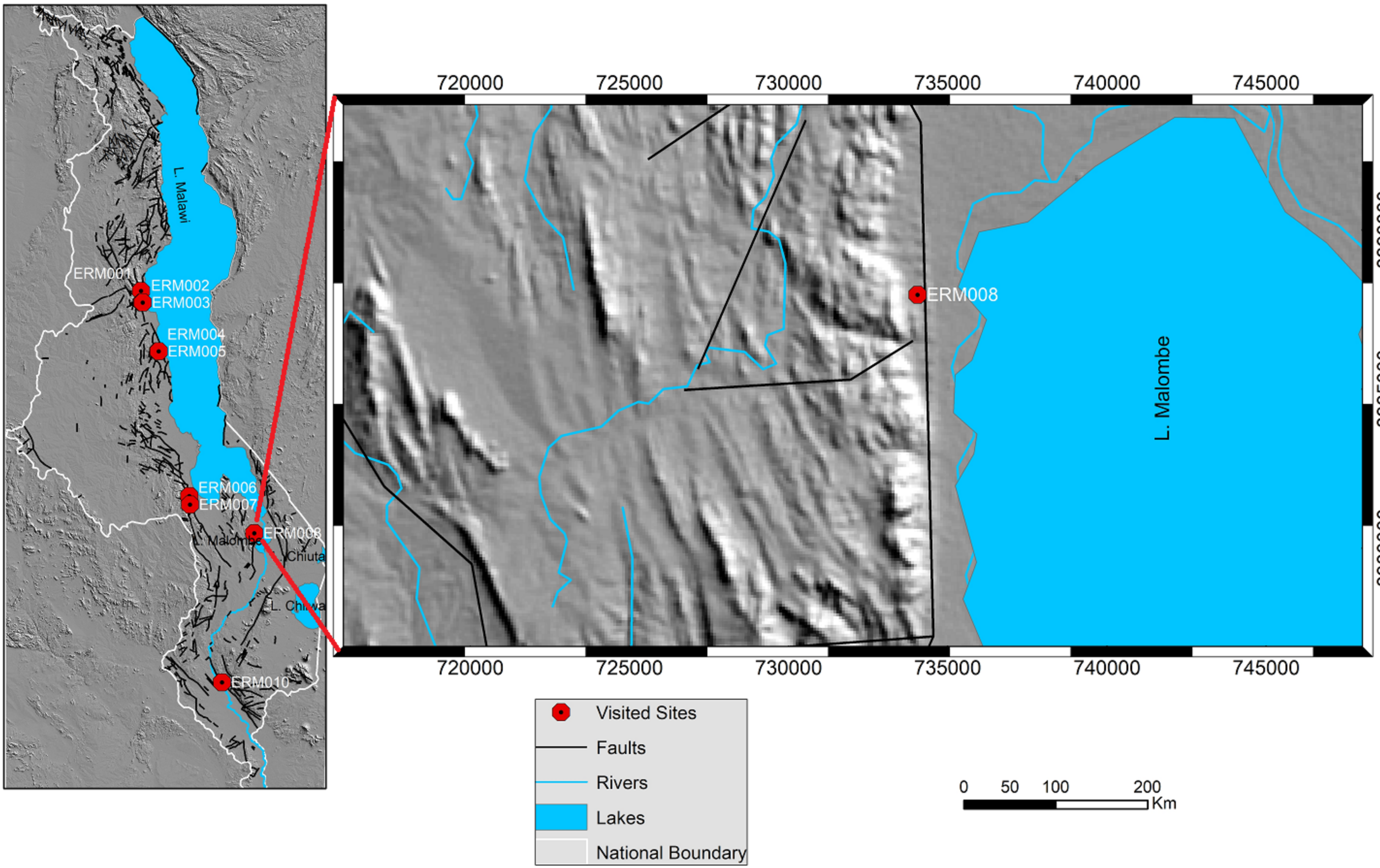
N
W
E
S
L. Malawi
ERM001
ERM002
ERM003
ERM004
ERM005
ERM006
ERM007
ERM008
ERM010
L. Malombe
L. Chiuta
L. Chilwa
720000
725000
730000
735000
740000
745000
8390000
8385000
8380000
Visited Sites
Faults
Rivers
Lakes
National Boundary
0
50
100
200
Km

Figure 10.

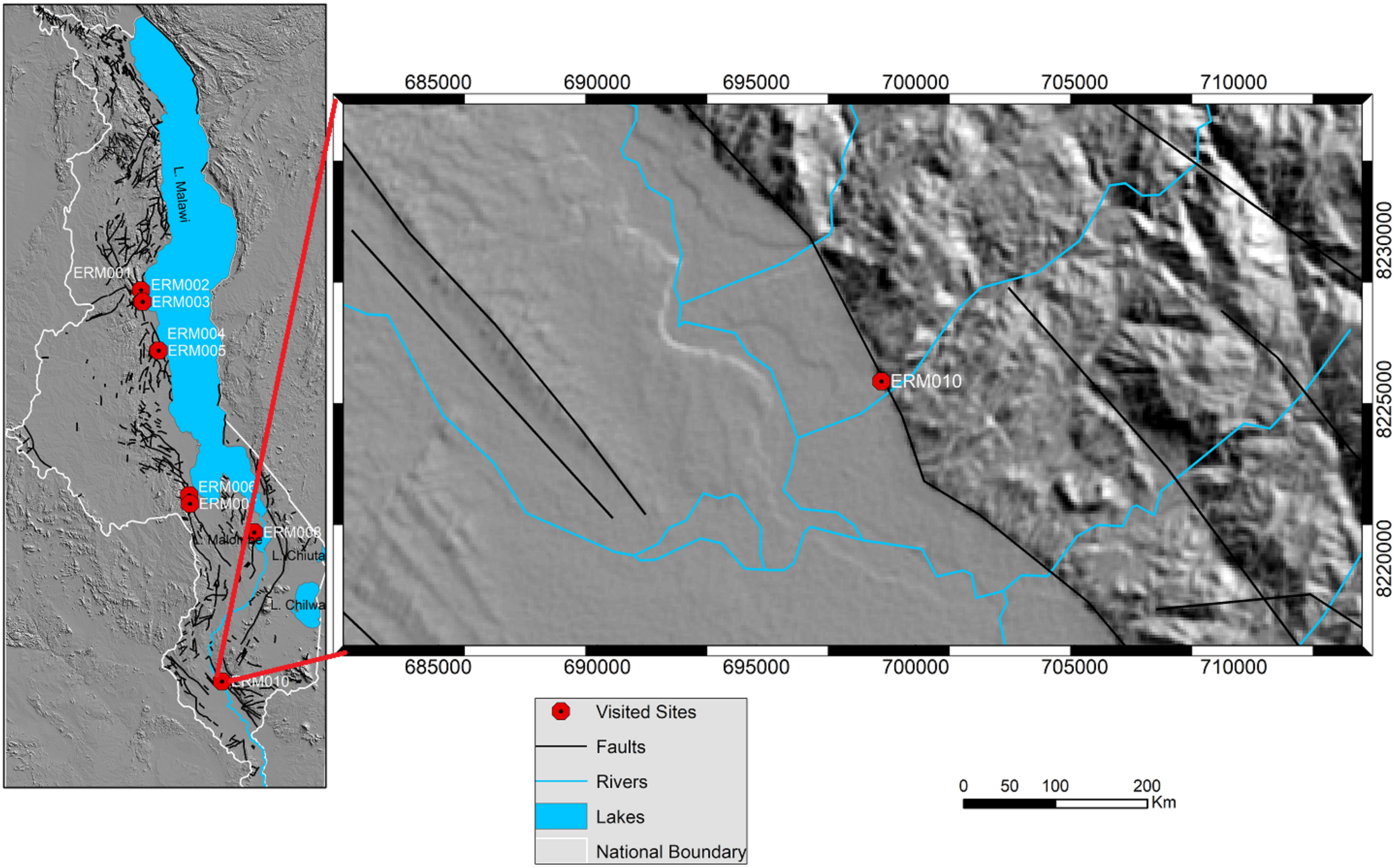
N
W
E
S
L. Malawi
ERM001
ERM002
ERM003
ERM004
ERM005
ERM006
ERM007
ERM008
L. Malombe
L. Chiuta
L. Chilwa
ERM010
685000
690000
695000
700000
705000
710000
8230000
8225000
8220000
Visited Sites
Faults
Rivers
Lakes
National Boundary
0
50
100
200
Km